Electronic Supplementary Material (ESI) for Physical Chemistry Chemical Physics.

Supplementary data for :

FAILURE MECHANISMS OF NANO SILICON ANODES: AN ELECTRODE POROSITY EVOLUTION MODEL

Silicon used in this study:

The active material we use in this work is made of Si nanoparticles. Its BET surface was found to be around 13 $m^2.g^{-1}$. In addition, XRD (Figure S1) and TEM (Figure S2) characterizations were carried out on this material.

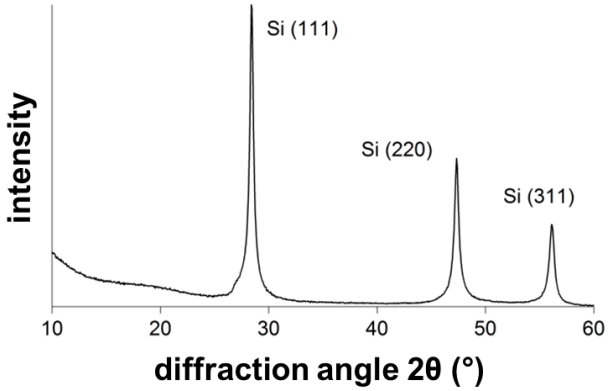

Figure S1. XRD diagram of the active material used in this study. The diagram was acquired on a Brücker D8 Advance diffractometer θ-θ configuration with a Cu anticathode.

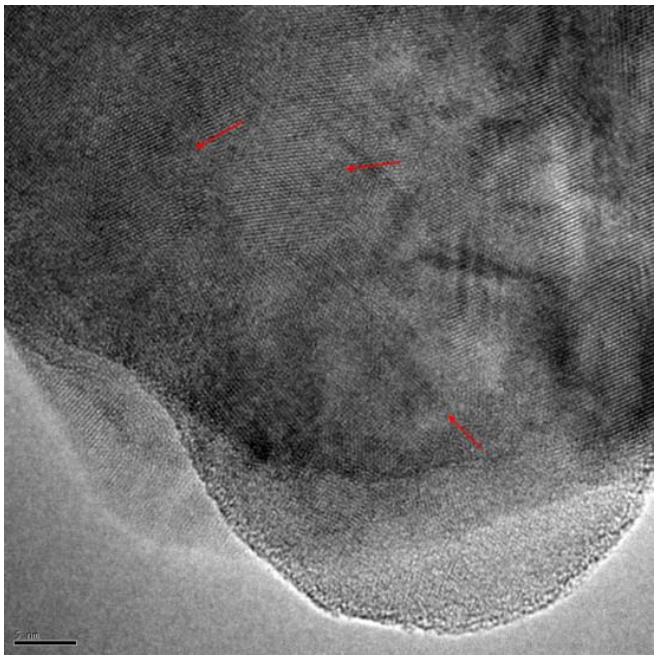

Figure S2. TEM image of a Si particle.

The Si nanoparticles are polycrystalline. The thickness of the oxide surface layer is found to be under 1 nm.

Mercury porosimetry analyses:

Hg porosimetry has been rarely used in the LIBs research field[1,2,3,4,5]. In this paper, mercury intrusion and extrusion measurements were achieved by using a Micromeritics Autopore equipment. The pressure range was scanned from 0.01 to 200 MPa which roughly corresponds to a pore size from ~200 µm to ~5 nm.

To increase the porous volume of the samples and therefore improve the measurements precision, a sample is made of several "pieces" of electrode. All the "pieces" of one sample are, of course, in the same state of aging. The total mass per sample is around 80 mg. As described in the paper, 3 samples were analyzed: before cycling, after 10 cycles, and after 100 cycles. For the "pieces" of electrode analyzed after cycling, before the measurement, they were washed twice in DMC inside the glove box (1 min per time). The "pieces" are then weighed (± 0.01 mg) and introduced in the sample holder (Figures S1 and S2). To keep, as much as we can, the samples from air exposure, the cup is covered with a plastic film and transferred from the glove box to the penetrometer.

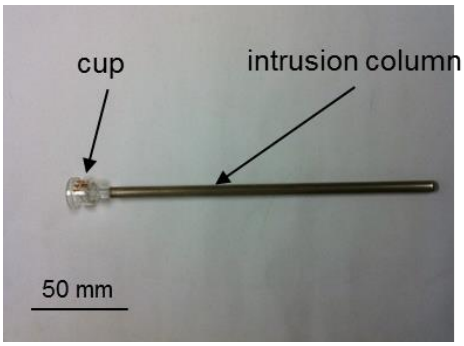

Figure S3. Picture of the sample holder used for the Hg porosimetry analyses.

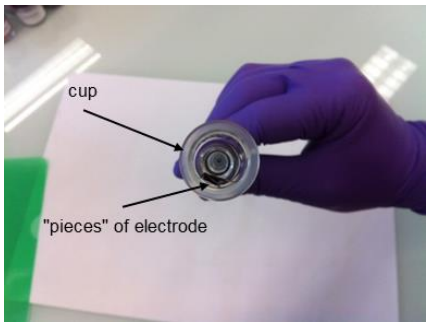

Figure S4. Picture of electrode "pieces" introduced in the cup.

Figure S5 shows the results obtained for (i) two samples made of "pieces" of pristine electrode, designated as "electrode try 1" and "electrode try 2" on the figure, and (ii) one sample made of "pieces" of current collector solely (copper), designated as "current collector only"; for the latter, the total mass is also equal to ~80 mg. The results obtained for "electrode try 1" and "electrode try 2" are very similar indicating that the analysis is reproducible. Two types of pores are clearly revealed: the first one, in blue, corresponds to a mercury intrusion at low pressure in very large pores (~100 µm).

[1] Carmier, D.; Vix-Guterl, C.; Lahaye, J. *Carbon* **2001**, *39*, 2181-2186.
[2] Maheshwari, P. H.; Nithya, C.; Jain, S.; Mathur, R. B. *Electrochim. Acta* **2013**, *92*, 55-63.
[3] Qi, X.; Blizanac, B.; DuPasquier, A.; Oljaca, M.; Li, J.; Winter, M. *Carbon* **2013**, *64*, 334-340.
[4] Lundblad, A.; Schwartz, S.; Bergman, B. *J. Power Sources* **2000**, *90*, 224-230.
[5] Lagergren, C.; Lundblad, A.; Bergman, B. *J. Electrochem. Soc.* **1994**, *141*, 2959-2966.

This porosity may be associated with mercury intrusion between the "pieces" of electrode. The second intrusion, in red, occurs when the pressure is equal to ~5 MPa, corresponding to a pore diameter of ~400 nm. This pore size is in good agreement with the SEM images of the electrode cross-section (Figure 5-a)) and thus can be related to the electrode porosity. The results obtained for the sample made of "pieces" of current collector confirm these hypotheses: only the intrusion at low pressure is observed.

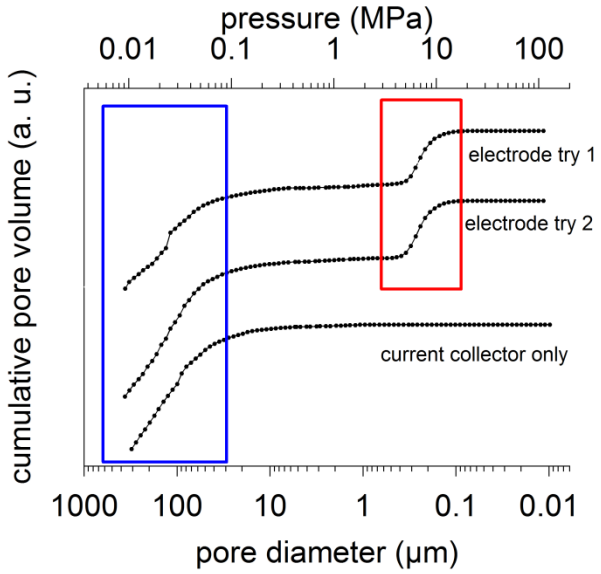

Figure S5. Mercury intrusion porosimetry analyses for (i) two samples made of pristine electrode "pieces" and (ii) one sample made of current collector.

Figure S6 shows the mercury intrusion and extrusion curves obtained on a sample made of "pieces" of electrode after 10 cycles. As it is said in the main article, the initial pore diameter at ~400 nm has disappeared: instead, two scales of porosity are observed at ~1 µm and under 100 nm. The extrusion curve reveals a trapped volume which can be related to a phenomenon of "ink bottle effect"[6].

[6] Leon y Leon, C. *Adv. Colloid Interface Sci.* **1998**, *76-77*, 341-372.

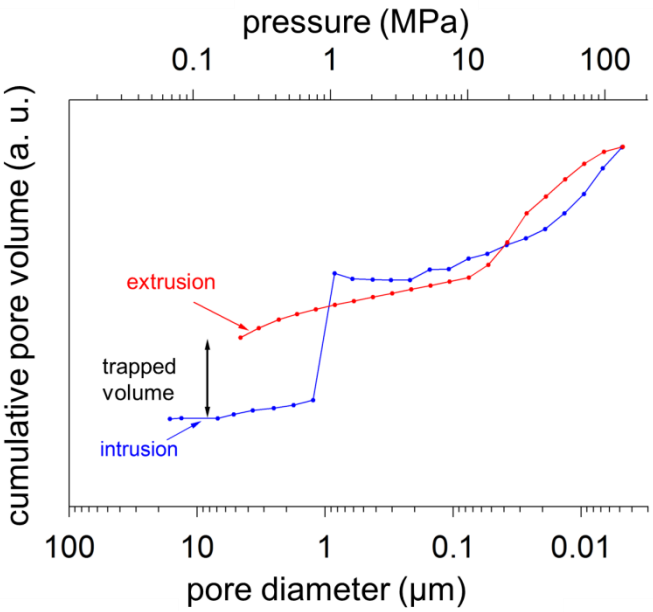

Figure S6. Mercury intrusion and extrusion curves obtained after 10 cycles.

Figure S7 shows the mercury intrusion and extrusion curves obtained after 100 cycles. The micrometric porosity is no longer observed. In addition, compared to the total pore volume, the trapped volume is bigger than that for the electrodes analyzed after 10 cycles. It can be related to an increase of the Si electrode tortuosity upon aging.

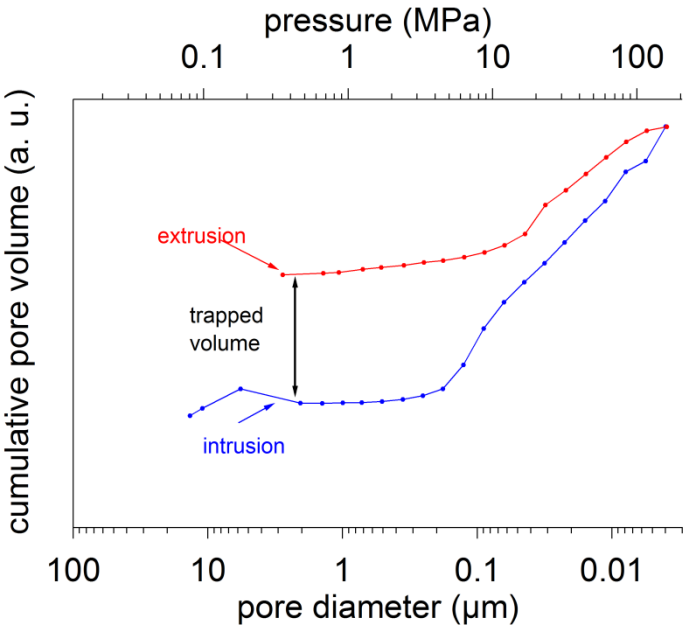

Figure S7. Mercury intrusion and extrusion curves obtained after 100 cycles.

The derivative curves are also interesting and clearly show the multi modal pore distribution (Figure S8).

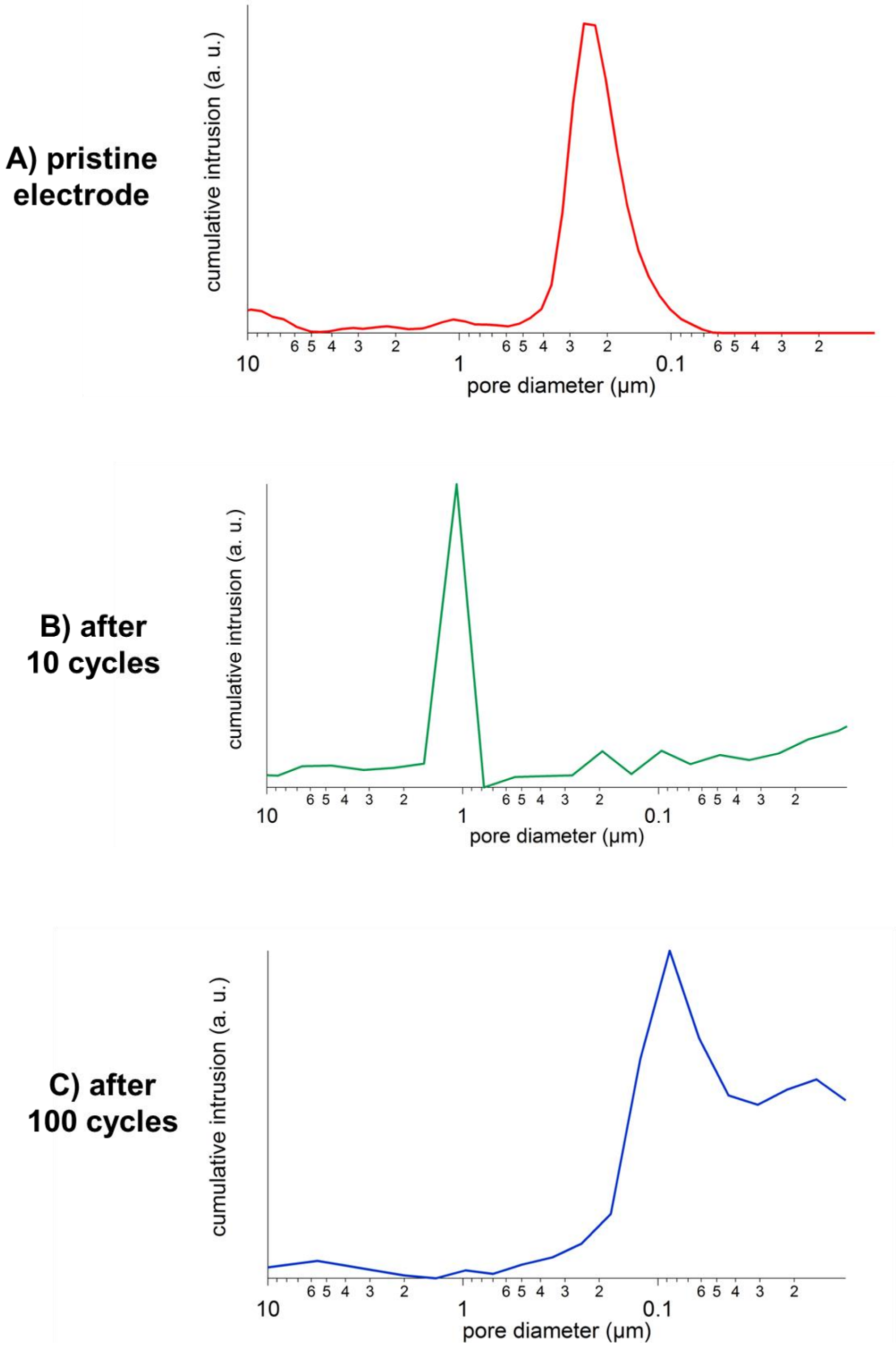

Figure S8. Mercury cumulative intrusion *vs* pore diameter upon cycling.

Impact of the first electrochemical cycle:

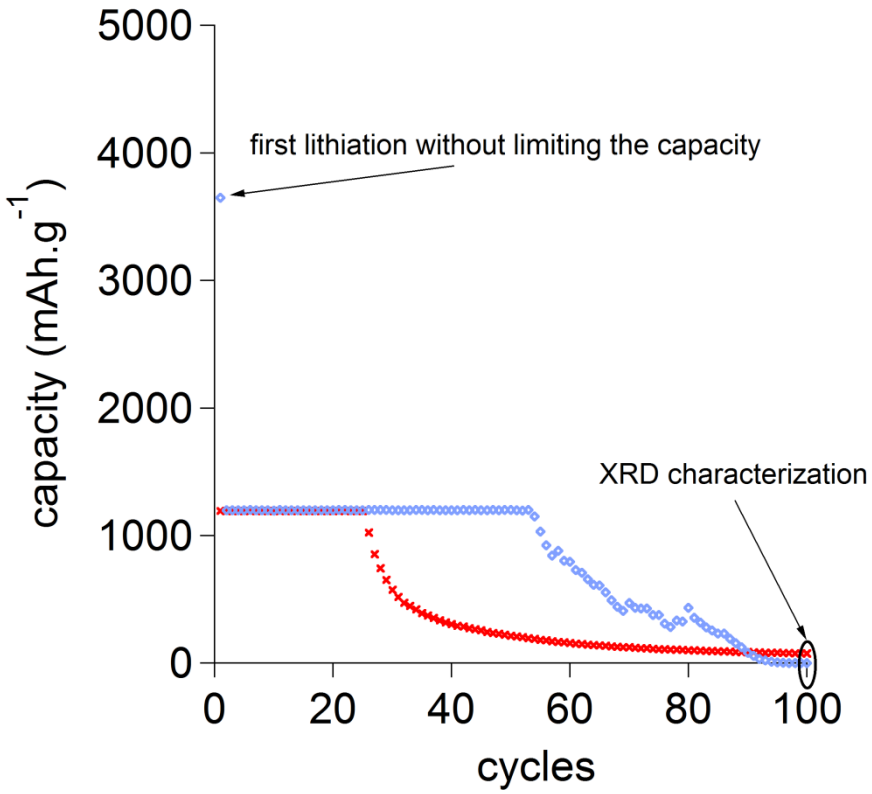

Figure S9. Evolutions of the discharge capacity *vs* cycle number for two Si electrodes. For the first electrode (x), the first discharge/lithiation capacity is limited to 1200 mAh.g^{-1}; for the second electrode (◊), the electrode is firstly fully lithiated/delithiated before limiting the discharge/lithiation capacity to 1200 mAh.g^{-1}.

Figure S9 shows the evolutions of the discharge capacity *vs* cycle number for both electrodes: (◊) with and (x) without a full first electrochemical cycle; this full cycle can be seen as a precycling of the Si electrode. When the capacity is not limited during the first cycle, the first discharge capacity is equal to 3800 mAh.g^{-1}; the capacity of 1200 mAh.g^{-1} is then maintained over 50 cycles. When no precycling is carried out and the discharge capacity is limited to 1200 mAh.g^{-1} since the first cycle, a capacity fading is observed after less than 30 cycles. To try to understand this difference of cyclability, both electrodes were analyzed by XRD after 100 cycles.

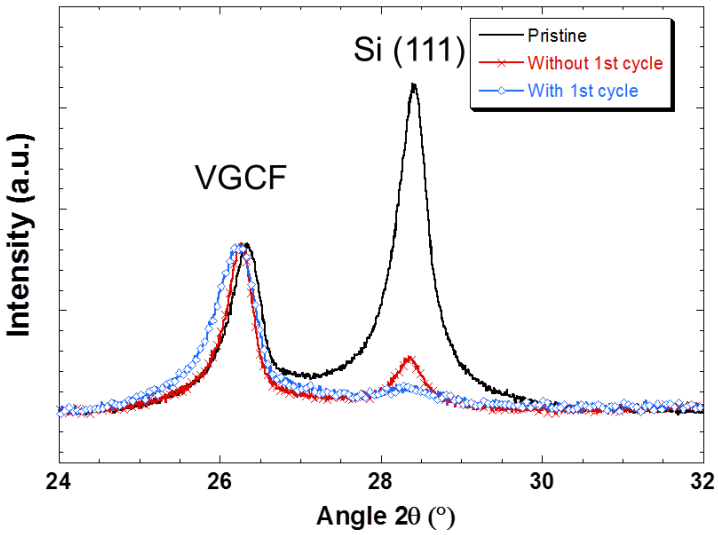

Figure S10. XRD diagrams of three Si electrodes: (-) pristine, (x) without precycling, and (◊) with precycling.

Figure S10 shows the XRD diagrams obtained for the (-) pristine electrode and after 100 cycles for two electrodes: (x) without and (◊) with precycling. Surprisingly, a signal which can be related to crystalline silicon is found for both Si electrodes analyzed after cycling. Indeed, silicon lithiation results in an amorphization of the active material[7]. Thus, the presence of crystalline silicon suggests that, for both electrodes, some of the silicon has never been lithiated during the first 100 cycles. The peak observed at 26.3° has been attributed to the carbon fibers or VGCF (Vapor Grown Carbon Fibers). For both electrodes analyzed after cycling, the quantity of crystalline silicon has been calculated by using the signal associated with the carbon fibers. This approach is based on two hypotheses: (i) the proportion of conductive agent is identical for the 3 analyzed electrodes and (ii) cycling does not affect the VGCF crystallinity. After 100 cycles, when a precycling is carried out, less than 3% of the initial crystalline silicon remains within the electrode; without precycling, this proportion is over 13%. We assume that, when a precycling is achieved, the discharge capacity of 3800 $mAh.g^{-1}$ (Figure S9) indicates that almost all the active material is lithiated and becomes amorphous during the first lithiation. On the contrary, when there is no precycling and the capacity is limited to 1200 $mAh.g^{-1}$ since the first cycle, only a fraction of the silicon is lithiated and becomes amorphous. During the following cycles, as the lithiation of amorphous silicon is easier than that of crystalline silicon[8], the amorphous silicon which has been lithiated previously is more likely lithiated. This cycling is responsible for a strong heterogeneity of the lithiation within the electrode and accelerates the degradation of the electrode electrochemical performances.

[7] Obrovac, M. N.; Christensen, L. *Electrochem. Solid-State Lett.* **2004**, *7*, A93-A96.
[8] Zhang, W. J. *J. Power Sources* **2011**, *196*, 13-24.

XPS analyses:

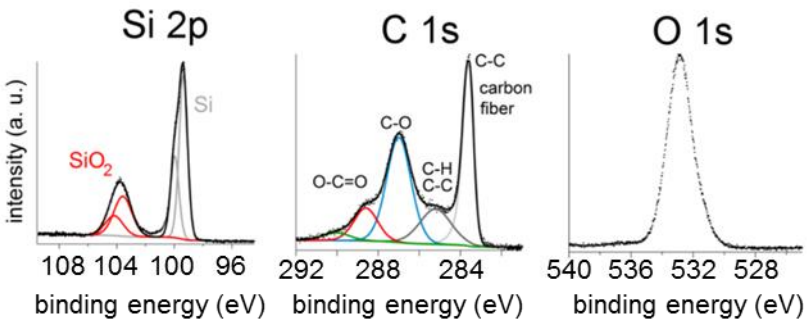

Figure S11. XPS spectra of the pristine electrode.

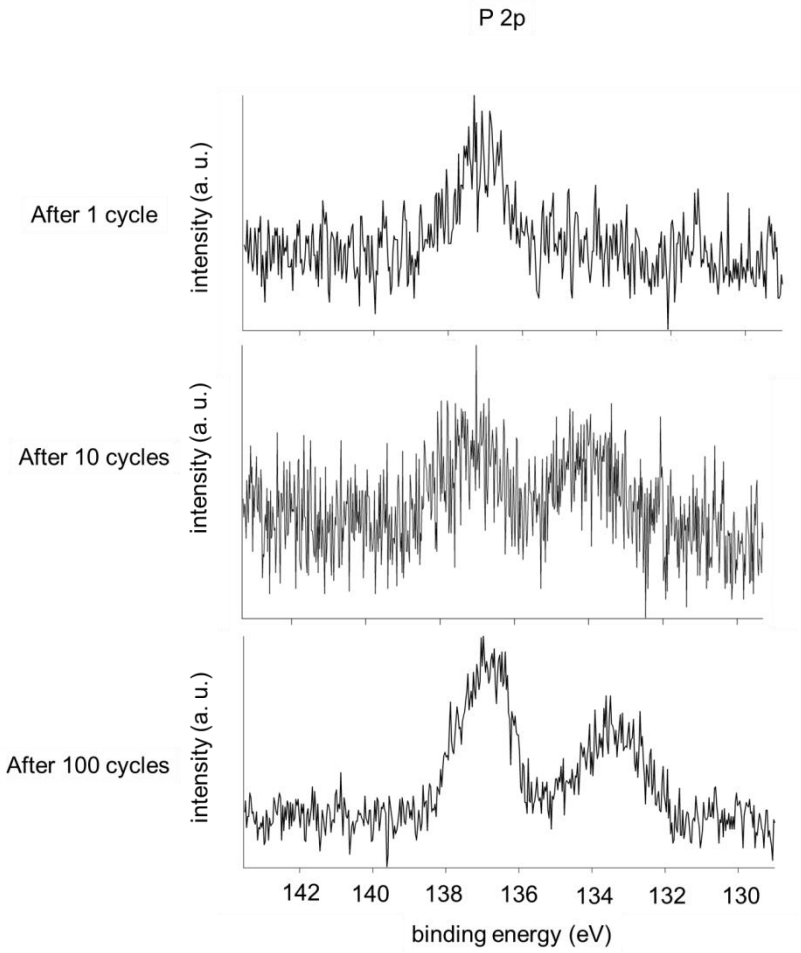

Figure S12. XPS spectra (P 2p core peaks).

FIB cross-sections

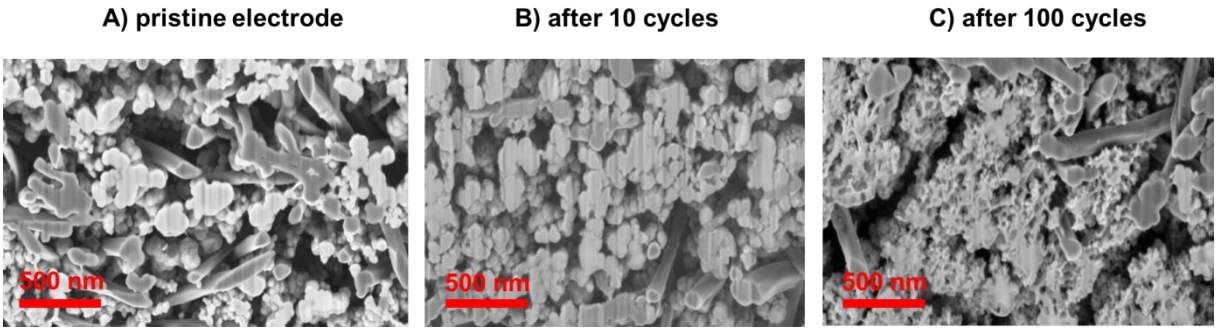

Figure S13. High-Resolution cross-sectional images: A) pristine electrode, B) after 10 cycles, and C) after 100 cycles.

Figure S13 shows HR SEM images of the Si electrode cross-section upon cycling. As it is written in the main paper (section 3.3.1), Si appears in very light grey and the carbon fibers in dark grey. The aggregation of the active material upon cycling is very clear on these images; after 100 cycles, these aggregates look very porous. In addition, it is interesting to note that the carbon fibers' morphology is rather stable.

Electrochemical Impedance Spectroscopy:

Based on de Levie's work[9] and considering that R_s (the electrolyte resistance) and Z (the pore's wall polarization) do not vary along the axis of the pore, if we apply, at the pore orifice, an alternating voltage, $e = e_0 \sin(\omega t)$, with angular frequency ω and small amplitude e_0 (so that the kinetics equations may be linearized), the impedance of one individual pore, Z_0, is thus defined by:

$$Z_0 = \frac{e_0}{i_0} = \sqrt{R_s Z}\,\coth\left(\sqrt{\frac{R_s}{Z}}L\right) \qquad \textbf{(I)}$$

If $Z = CPE_x = \frac{1}{Q(j\varpi)^{\alpha}}$ (considering a totally blocking electrode/confined electrolyte interface due to a mostly invariant lithium concentration inside the pores), the subsequent equivalent transmission line is then:

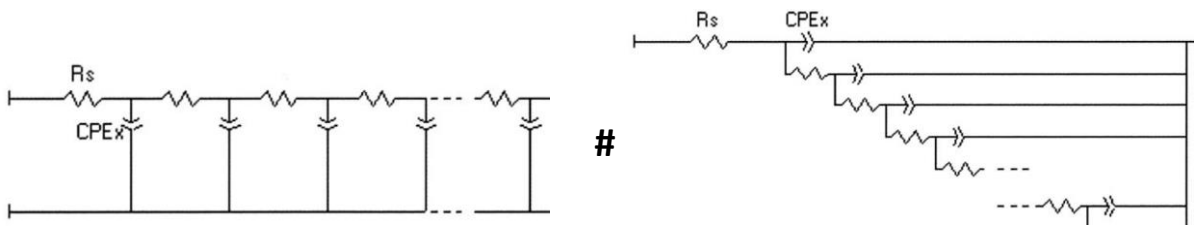

[9] de Levie, R. *Advances in Electrochemistry and Electrochemical Engineering*, Wiley Interscience Ed: New York, 1967.

In semi-infinite condition ($L \to \infty$), and with $\alpha = 1$ (CPE_x is then a pure capacitance) the pore behaves like a Warburg element, with a 45° phase shift between potential and current. This behaviour is not surprising in view of the subsequent close analogy between our pore's equivalent circuit and a standard planar diffusion *R//C* transmission line.

We try now to go further and take into account the variation of R_s and Z along the pore in order to estimate Li diffusion coefficients.

In order to depict our system, as simple as possible, a simplification is introduced in our diffusion model: one-dimensional concentration profile. Actually, neglecting here radial gradient of concentration (with respect to the main axial one) is considered to be relevant enough for narrow cylindrical pores in the absence of forced convection.

In that case, second Fick's law allows the expression of one-dimensional concentration profile:

$$\frac{dC}{dt} = D\frac{d^2C}{dx^2} - KC \qquad \textbf{(II)}$$

Where *C* is, here, the lithium ions concentration inside pores, *D* the diffusion coefficient and *K* can be regarded as a pseudo-homogeneous rate constant accounting for the irreversible "consumption" of mobile lithium inside pores (*ie* immobilization of lithium ions through the SEI formation).

In a pore, the boundaries conditions imposed:

$x = 0$ $\qquad C(x) = C_0$

$x = L$ $\qquad \frac{dC}{dx} = 0$

So that, in steady-state condition:

C(x) do not depend on time and eq(II) gives $C(x) = C_0 \dfrac{\cosh\left[\sqrt{\frac{K}{D}}(x-L)\right]}{\cosh(\sqrt{\frac{K}{D}}L)}$ **(III)**

The overall flux of lithium ions inside the pores can thus be calculated as follows:

$$J = -D\left(\frac{dC}{dx}\right) = C_0\sqrt{KD}\tanh\left[\sqrt{\frac{K}{D}}L\right] \qquad \textbf{(IV)}$$

and the corresponding steady-state current is $I = F.J = FC_0\sqrt{KD}\tanh\left[\sqrt{\frac{K}{D}}L\right]$ **(V)**

In semi-infinite condition ($L \rightarrow \infty$), from eq.(V), we can estimate the maximum mobile lithium ion's penetration depth, λ, under a constant current load I_0:

$$\lambda = \sqrt{\frac{D}{K}} = \frac{FC_0 D}{I_0} \qquad \textbf{(VI)}$$

Now, in non-steady state conditions, *ie* when lithium ions concentration inside a pore is time and space dependent (following second Fick's law), the response to a small sine wave perturbation, $e = e_0 \sin(\omega t)$, can be expressed from the Taylor expansion of eq.(II) limited to first order terms:

$$\frac{d\Delta C}{dt} = D\frac{d^2\Delta C}{dx^2} - K\Delta C - \frac{dK}{de}C(x)\Delta e = j\omega\Delta C \qquad \textbf{(VII)}$$

Keddam *et al*[10] has then demonstrated that, in these particular conditions, the impedance, Z_0, of one individual pore is expressed as:

$$(Z_0)^{-1} = \frac{dK}{de}FC_0\sqrt{\frac{D}{K}}\tanh\left(\sqrt{\frac{K}{D}}L\right) + \frac{K\frac{dK}{de}FC_0}{j\omega}\left[\sqrt{\frac{D}{K+j\omega}}\tanh\left(\sqrt{\frac{K+j\omega}{D}}\right) - \sqrt{\frac{D}{K}}\tanh\left(\sqrt{\frac{K}{D}}\right)\right] \qquad \textbf{(VIII)}$$

In semi-infinite condition ($L \rightarrow \infty$), with $K \neq 0$ and with $\alpha = 1$ (CPE_x is then a pure capacitance), it is interesting to remark that the pore behaves now like a *R//C* circuit (the contribution of the axial diffusion appears as a semi-circle in the Nyquist impedance representation) since: $\underset{\omega\rightarrow\infty}{Lim}(Z_0) = R_{HF}$ and $\underset{\omega\rightarrow 0}{Lim}(Z_0) = R_{BF}$.

However, the pseudo-homogeneous rate constant, *K*, should be very small in our case (few lithium ions "consumption" through the SEI formation since the coulombic efficiency remains as high as 99%, even after 100 cycles), so that it leads to $\underset{K\rightarrow 0}{Lim}(R_x) \rightarrow \infty$ (in the corresponding electrical equivalent circuit) and one finally recovers the first model (blocking pore's wall).

From an experimental point of view, our system is probably in-between (smooth curvature of the classical Warburg domain with a trend, upon ageing, to progressively become resistive), but, for simplicity, we have chosen to fit the experimental data with the first electrical equivalent circuit (as the data collected are rather consistent with a mostly blocking pore's wall), with $Z = CPE_x = \frac{1}{Q(j\varpi)^{\alpha}}$.

At last, the boundary impedance (current collector/electrode interface) is chosen as a non-infinite one ($Z_{boundary} = CPE_t = \frac{1}{Q_t(j\varpi)^{\alpha}}$) to take into account the very low frequencies dispersion. The $Z_{boundary}$ is at the end of the resistive channel (referred to confined electrolyte), so that $Z_{boundary}$ is neither in parallel nor in series with the "bulk" transmission line. In that specific case, the local impedance

[10] Keddam, M.;Rakotomavo, C.; Takenouti, H. *J. Applied Electrochem.* **1984**, *14*, 437.

$Z_{boundary}$ cannot modify the highest frequencies response of the transmission line (pore's behaviour), which remains determined by the "bulk" properties[11].

[11] Bisquert, J. *Phys. Chem. Chem. Phys.* **2000**, *2*, 4185.